Defect Mitigation in Area-Selective Atomic Layer Deposition of Ruthenium on Titanium Nitride/Dielectric Nanopatterns

Job Soethoudt[1,2], Hubert Hody[2], Valentina Spampinato[2], Alexis Franquet[2], Basoene Briggs[2], Boon Teik Chan[2], Annelies Delabie[1,2*]

1 Department of Chemistry, KU Leuven (University of Leuven), 3001, Leuven, Belgium

2 Imec, Kapeldreef 75, 3001, Leuven, Belgium

*Annelies.Delabie@imec.be

ABSTRACT: Area-Selective Deposition (ASD) receives increasing attention as a bottom-up approach for nanoelectronic device fabrication. Uptake of ASD is however limited by defects, which manifest as undesired particle growth on the non-growth surface. We demonstrate a defect mitigation solution for Ru ASD on TiN/SiO_2 nanopatterns by making use of the size-dependent Ru nanoparticle reactivity. During the initial stages of 1-(ethylbenzyl)-1,4-(ethylcyclohexadienyl)ruthenium and oxygen (EBECHRu/O_2) Atomic Layer Deposition on dielectrics, Ru particles are too small to catalytically dissociate oxygen, and their growth is suppressed. This phenomenon creates an ASD process window in which particles can be completely etched while retaining the integrity of the ASD pattern on a TiN growth surface. Decreasing the ALD temperature strongly suppressed defect growth, which can be used to expand the process window for ASD. The ASD process window is confirmed by Self-Focusing Secondary Ion Mass Spectrometry (SF-SIMS) with its low limit of detection while analyzing 10^4 structures simultaneously. No defects are detected for Ru ASD on 36nm TiN/SiO_2 patterns by SF-SIMS. We apply the Ru ASD process for bottom-up block patterning and obtain functional hardmask patterns on 300mm wafers. The approach followed in this work can produce defect-free ASD processes for a wide variety of applications.

Area-Selective Deposition (ASD) has received significant attention for a multitude of bottom-up patterning applications[1–4]. In ASD, chemical selectivity is exploited to deposit a material on one surface type (the growth surface) selectively to another (the non-growth surface). Amongst others, ASD is of interest for self-aligned processing and the bottom-up filling of ultrasmall 3D features in nanoelectronic device fabrication. Filling of features is conventionally performed by deposition over the entire substrate, resulting in excess material deposition on the areas surrounding the features of interest. This excess material then needs to be removed by etch or Chemical Mechanical Polishing (CMP), introducing additional process steps. Furthermore, the fill performance of conventional methods becomes increasingly challenged by pinch-off and void formation due to ever decreasing feature sizes[5], and significant differences in filling behavior between wide and narrow features are observed. ASD could address all of these issues, resulting in a uniform bottom-up deposition in 3D features. As a result, significant effort has been made to demonstrate ASD of a variety of materials for a broad range of applications[2–4,6–12].

Nevertheless, selective deposition on the growth surface occurs simultaneously with unwanted inhibited deposition on the non-growth surface. This growth on the non-growth surface is referred to as defectivity, and often manifests as particle growth[9,10]. Typically an ASD process window is defined as the process time or amount of cycles in which deposition on the non-growth surface remains below a pre-defined limit[13–15]. This limit is often defined as the Limit Of Detection (LOD) of the method used to characterize defectivity, but can also originate from the application requirements. Self-Focusing Secondary Ion Mass Spectrometry (SF-SIMS) is well-suited for defect characterization in ASD due to the capability to analyze large patterned areas containing over 10^4 structures, and the superb limit of detection of Time-of-Flight Secondary Ion Mass Spectrometry (ToF-SIMS) which ranges between 10^6-10^{11} at cm^{-2} [16–18]. The mechanism of defect formation and growth depends on the deposition process used, and models have been developed for particle growth of both dielectrics[19,20] and metals[21,22]. Since defectivity is a major challenge for ASD uptake in industry, considerable efforts have been made to expand the ASD window, either by prolonging growth inhibition[6,10], letting defects diffuse from the non-growth to the growth surface[23], or by removal of defects after ASD[4,15]. The latter is typically achieved by adding an etch step.

However, since the etch step also attacks the ASD-grown film, this strategy can only be applied when the defects are smaller than the selectively grown film or when the etch rate for defects exceeds that of the selectively grown film. During Atomic Layer Deposition (ALD) of dielectrics, islands grow radially each cycle at the same rate as films[19]. During ALD of metals, diffusion and aggregation during island growth can even result in particles which are larger compared to films grown on the growth surface[21]. This implies that even though less material is typically deposited on the non-growth compared to the growth surface, the individual particles cannot be fully etched without also removing films grown on the growth surface. Nonetheless, when the defect growth mechanism is understood it may be exploited to facilitate defect mitigation.

The surface dependence and growth mechanism of 1-ethylbenzyl-1,4-cyclohexadienylruthenium (EBECHRu)/O_2 ALD can be used for Ru ASD on metals with respect to dielectrics. A strategy

to mediate defectivity on dielectrics can be proposed based on the growth mechanism during the initial stages of ALD[22]. In the initial stages of Ru growth on Si-CH₃ terminated dielectrics, the mechanism is governed by (1) extremely slow deposition of adatoms on the Si-CH₃ terminated surface, and (2) diffusion and aggregation of these adatoms into larger particles. As long as those particles remain smaller than the critical diameter of ~0.85nm, catalytic oxygen dissociation does not occur on the particle surface. As such, direct ALD on the particle surface is suppressed which limits the growth of large nanoparticles on the non-growth surface. This size-dependent growth can be exploited in a post-deposition etch step. Diffusion of Ru species on the dielectric surface can also play a role in ASD, especially when the pattern dimensions become comparable to or smaller than the species diffusion length. This phenomenon is exploited amongst others in selective epitaxial growth[23]. Finally, EBECHRu/O₂ ALD is enhanced on TiN surfaces at 325°C due to continuous segregation of $Ti(O,N)_x$ surfactants to the top surface[24]. This surfactant-mediated growth leads to an increased steady deposition rate on TiN compared to Ru, and is therefore advantageous for ASD.

In this paper we design a defect mitigation strategy for Ru ASD based on this growth mechanism. We will demonstrate that the delay in initial growth due to size-dependent particle reactivity can be exploited to etch the small initial particles while minimizing attack of the selectively grown film. Additionally, the diffusion and aggregation of Ru particles can be limited by lowering the ALD temperature in order to keep particles below the critical size. We investigate Ru ASD on TiN with respect to SiO₂, which is relevant for Tone Inversion (TI) patterning. TI is an important patterning technology in nanoelectronic manufacturing[25–29], and is one of the applications where ASD can solve challenges posed by the decreasing feature dimensions[30]. We investigate the high end of the ALD temperature window (325°C) to make use of the enhanced Ru growth on TiN[24], and the low end of the ALD temperature window (225°C) to minimize Ru particle growth by diffusion and coalescence. First, differences in growth behavior between non-patterned surfaces and those in TiN/SiO₂ nanopatterns are identified and explained. Next, after characterizing the growth of defects on nanopatterns, we determine the efficacy of the proposed defect mitigation strategy using the low SF-SIMS LOD)to monitor defectivity reduction in large patterned areas containing over 10^4 structures. Finally, the Ru ASD process is used to enable bottom-up TI patterning in 36nm structures on 300mm wafers.

Results and Discussion

Area-selective Ru film growth on TiN in TiN/SiO₂ nanopatterns

Since ALD is governed by surface reactions, the chemical and physical properties of each exposed surface strongly affect the growth behavior. As such, growth behavior can differ significantly between large-area substrates and nanopatterns, for instance due to the chemical and physical surface modifications induced by patterning, as well as the feature sizes and topography in nanopatterns. The latter may become increasingly important for diffusion-mediated deposition when the diffusion length approaches the dimensions of the pattern. To understand the impact of nanopatterned substrates on ALD, we first compare the Ru growth behavior on non-patterned surfaces and TiN/SiO₂ nanopatterns at 325°C, the high end of the ALD temperature window, to make use of the enhanced Ru growth on TiN[24] and to assess the impact of Ru particle diffusion on dielectrics in nanopatterns. All substrates used in this study are treated with Dimethylamino-Trimethylsilane (DMA-TMS) which selectively inhibits growth on dielectrics by rendering the SiO₂ surface -Si(CH₃)₃ terminated[7,8,22]. Ru ASD on TiN vs

SiO₂ is achieved on both line and hole patterns, as a Ru film is selectively deposited on TiN while the inhibited growth on SiO₂ results in particles (Figure 1a). The Ru layer thickness on TiN inside the holes was compared to results on large-area non-patterned TiN substrates, as diffusion of Ru particles from the non-growth area to the growth area could affect the Ru layer thickness on the growth area, similarly to what is observed in selective epitaxial growth[23]. After 83 Ru ALD cycles approximately 4nm film growth is observed on TiN in all investigated features ranging from 36nm-90µm, which agrees with the 4nm film thickness observed on non-patterned TiN substrates (Figure 1b). As no differences in Ru film thickness are observed at different feature sizes, and the Ru layer thickness near the TiN/SiO₂ interface is the same as in the middle of large TiN features, we conclude that diffusion of Ru defects on SiO₂ does not significantly affect the Ru layer thickness on TiN. We attribute this to the limited diffusion length of Ru particles compared to the vertical dimensions of the sidewall. Single Ru adatoms have a ~16nm diffusion length, and this diffusion length decreases by a factor $k^{-8/3}$ for a particle consisting of k atoms[22]. As a result, DMA-TMS/EBECHRu/O₂ ASD process produces a uniform layer thickness on TiN which appears independent of feature size over the investigated feature size range. A notable impact of surface diffusion is expected for smaller features with dimensions equal to or below the aforementioned diffusion length, as the probability that defects are captured by the growth surface increases. Using surface diffusion as a defect mitigation strategy is therefore expected to become attractive for this deposition process as feature dimensions of nanostructures decrease.
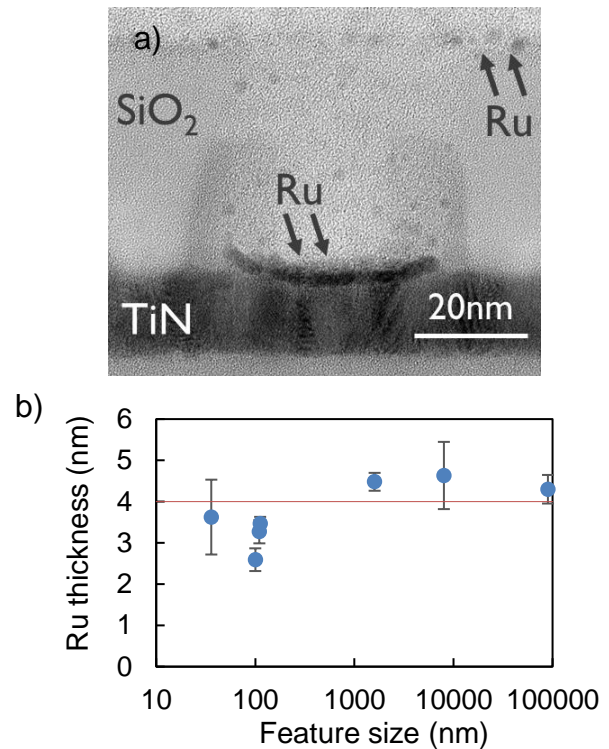
Figure 1: Evaluation of Ru thickness grown selectively on TiN at 325°C. a) cross-view Transmission Electron Microscopy (TEM) image of Ru ASD inside a 36nm feature after 83 cycles of Ru ALD. Both the ASD Ru film on TiN and the Ru particle defects on SiO₂ can be observed. b) Ru layer thickness on TiN inside hole patterns of 36nm-90µm after 83 cycles of Ru ALD. The red line corresponds to the Ru film thickness on large-area non-patterned TiN substrates after 83 Ru ALD cycles and is provided as reference.

2

Ru growth behavior on TiN/SiO₂ nanopatterns

We now investigate the growth evolution of Ru defects on nanopatterns to determine the impact of patterning on the surface, as well as the impact of topography and feature size. The Ru particle growth on the SiO$_2$ surfaces is studied on the line patterns, as these patterns contain large areas for both the top and sidewall SiO$_2$ surface on which particle growth can be analyzed (Figure 2a-c). Inhibited particle growth is observed on both top and sidewall, resulting in high areal densities of 10^{11}-10^{12} particles per cm^2. During diffusion-mediated growth processes, surface species may move from the non-growth to the growth surface, resulting in a depletion zone on the non-growth surface which depends on the species diffusion length[23]. Ru adatom deposition is irreversible during EBE-CHRu/O$_2$ ALD, which means that the diffusion length effectively corresponds to the mean free path of a Ru adatom diffusing over the surface before aggregation. While EBECHRu/O$_2$ ALD displays diffusion-mediated growth on dielectric surfaces, the diffusion length is limited (~16nm for single atoms on Si-CH$_3$ terminated dielectrics, and lower for particles consisting of multiple atoms)[22]. As such, the depletion zone is small compared to the 70nm vertical dimension of the SiO$_2$ surface adjacent to the TiN growth surface, and no significant depletion is observed visually in Scanning Electron Microscopy (SEM) for these structures (Figure 2c). One might observe different behavior on surfaces with an enhanced Ru species diffusion length, or when the nanopattern feature size becomes lower compared to the diffusion length.

The Ru particle density is quantitatively different on the top and sidewall SiO$_2$ (Figure 2d,e). While the growth evolution on the sidewall is comparable to that on non-patterned DMA-TMS treated SiO$_2$, growth proceeds more rapidly on the SiO$_2$ top surface. Top and sidewall surface originate from the same initial SiO$_2$ layer, but both surfaces experienced different process chemistries during pattern fabrication. Specifically, the sidewall surface was generated by etching with CF$_x$ based chemistry, while the top surface was covered with spin-on-carbon (SOC) which was stripped with an O$_2$ plasma afterwards. To assess the impact of these steps on the Ru growth behavior, large-area non-patterned SiO$_2$ substrates were exposed to the CF$_x$ etch and subsequent clean chemistry used during pattern fabrication, while other SiO$_2$ substrates were covered with SOC which was subsequently removed using the same strip procedure used during patterning. When these substrates were exposed to DMA-TMS and subsequent Ru ALD, only the SOC and O$_2$ plasma strip treated SiO$_2$ surfaces behaved differently compared to pristine SiO$_2$ (Figure 2f). While on as-deposited and CF$_x$-treated SiO$_2$ defect densities of $5 \cdot 10^{11}$ were observed, the SOC and O$_2$ plasma strip treated SiO$_2$ rapidly displayed over $1.5 \cdot 10^{12}$ defects. The higher defect density on the latter surface results in a more rapidly increasing coverage and faster agglomeration. Figure 2e shows the evolution of defect density with ALD cycle number, which initially increases as new particles are generated and decreases again as particles agglomerate to cover the SiO$_2$ surface. On as-deposited and CF$_x$ treated SiO$_2$ this happens after 100-150 cycles, while for SOC and O$_2$ plasma strip treated surfaces agglomeration occurs already after 67 ALD cycles. The top surface patterning is therefore expected to affect Ru growth behavior. A possible reason could be that carbon residues from the SOC layer enhance Ru adatom deposition on the top surface with respect to the sidewall. Enhanced atom deposition means that more material is available for diffusion and aggregation, and that particles reach critical size more rapidly. Ru deposition occurs faster on particles above critical size, explaining how enhanced Ru adatom deposition results in even more strongly enhanced Ru areal density. Higher particle density could also result from top surface roughening by the directional ion bombardment used to strip the SOC[31,32]. Specifically, surface roughening could limit Ru particle diffusion and aggregation resulting in a higher particle density. The latter mechanism would however limit particle size and therewith also limit the total amount of Ru deposited, contrary to what is observed in Figure 2e. We therefore expect the deposition enhancement by SOC residues to play a more prominent role in the differences observed between top and sidewall surface. To summarize, no impact of pattern dimensions on the growth behavior is observed, as pattern dimensions are still large compared to the Ru species diffusion length. However, the nanopattern fabrication does affect the growth behavior as the SiO$_2$ top surface patterning results in higher defect densities as compared to as-deposited SiO$_2$.

f)
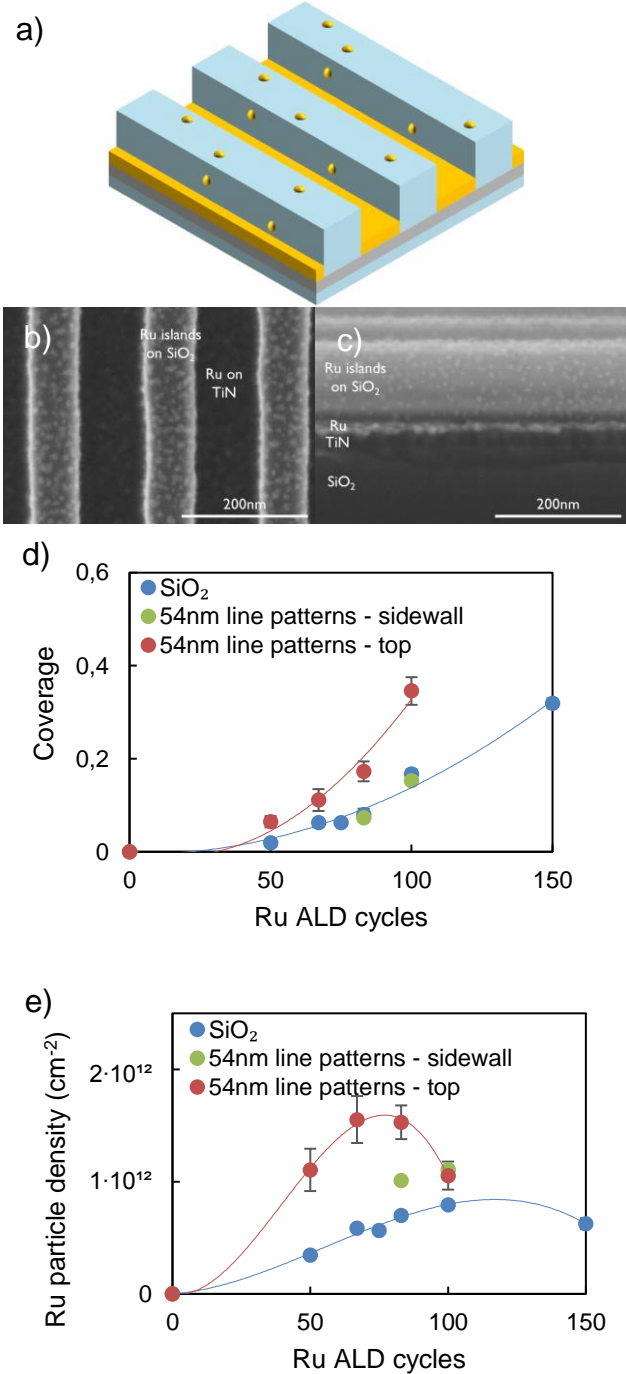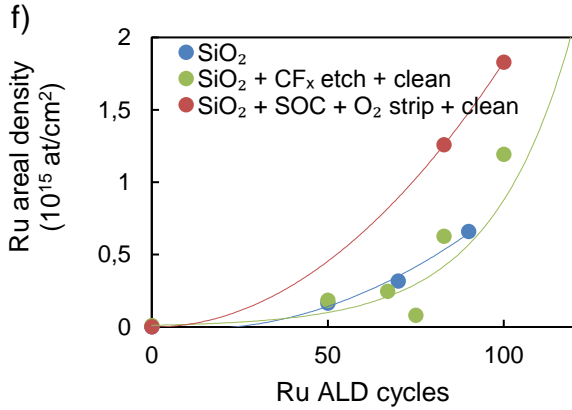
Figure 2: Evaluation of defectivity during Ru ASD at 325°C on TiN/SiO$_2$ line patterns. a) layout of the substrate after ASD of Ru (gold) on TiN (grey) selective to SiO$_2$ (blue) b) top-view SEM of Ru particles on the SiO$_2$ top surface after 83 cycles of Ru ALD c) cross-view SEM of Ru particles on the SiO$_2$ sidewall after 83 cycles of Ru ALD d) Ru coverage on SiO$_2$ in the TiN/SiO$_2$ line patterns as determined by SEM e) Ru particle density on SiO$_2$ in the TiN/SiO$_2$ line patterns as determined by SEM f) Ru areal density on SiO$_2$ blanket substrates exposed to various patterning chemistries as determined by Rutherford Backscattering Spectrometry (RBS)

SF-SIMS for defect analysis during ASD

Before investigating Ru defect mitigation on TiN/SiO$_2$ nanopatterns, the sensitivity of SF-SIMS towards Ru ASD defects is investigated and compared to that of SEM. The evolution of defect growth can be observed on the SiO$_2$ top surface in SEM (Figure 3a-c). The 36nm hole patterns were patterned using the same chemistries as the line patterns studied earlier, and while the particle growth on the sidewalls could not be quantified due to the geometry and small dimensions of the pattern, the growth behavior on the top surface is quantitatively comparable to that on the top surface of the line patterns. Due to its low LOD and low probe depth, ToF-SIMS is known to be among the most surface-sensitive characterization techniques. Furthermore, the analysis area can be large containing many structures, making the characterization less susceptible to local variability. However, a major challenge consists of finding an ion which (i) is unique for the feature of interest (in this case the SiO$_2$ non-growth surface), and (ii) is detected with sufficient yield[17,18]. For defect analysis in Ru ASD on TiN/SiO$_2$ nanopatterns, Ru defects on SiO$_2$ need to be distinguished from the Ru layer on TiN. In SF-SIMS this distinction is made by detecting cluster ions which originate specifically from undesired Ru growth on SiO$_2$. Therefore, an ion type that originates only from a Ru defect on SiO$_2$ should contain both Ru and Si. A variety of Ru-Si containing clusters was investigated on the 36nm TiN/SiO$_2$ hole patterns after Ru ASD at 325°C, and among those RuSiO$^+$ showed the highest yield. As a consequence, the RuSiO$^+$ ion was selected as a signature for Ru defectivity on SiO$_2$. To determine whether the ion yield is sufficient for defect metrology, SF-SIMS using RuSiO$^+$ was compared to SEM in terms of capability to detect defects. SEM can detect defects on the 36nm TiN/SiO$_2$ patterns after 42 and 83 Ru ALD cycles, as observed in the second and third image in Figure 3a. However in the first image corresponding to 21 Ru ALD cycles, no defects are observed in SEM after Ru ASD. In contrast, SF-SIMS is able to detect defectivity for all conditions (Figure 3d). These results show that SF-SIMS is more sensitive towards Ru defectivity on SiO$_2$ compared to SEM, and will therefore be used to

evaluate the efficacy of the defect removal strategy in the next sections.
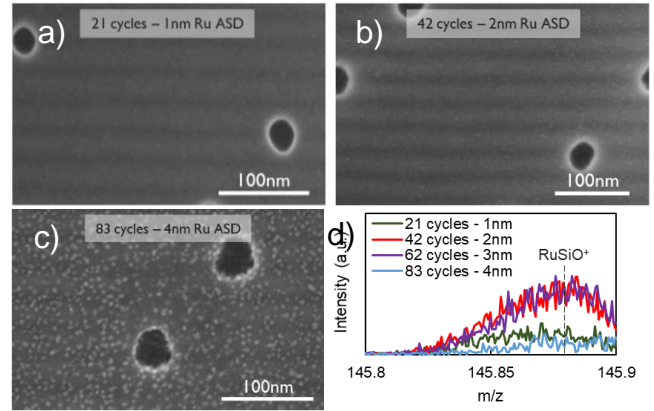
Figure 3: Top-down SEM of 36nm TiN/SiO$_2$ hole patterns after a) 1nm (21 cycles), b) 2nm (42 cycles), and c) 4nm (83 cycles) Ru ASD at 325°C. d) SF-SIMS can detect Ru defectivity on SiO$_2$ for all investigated numbers of Ru ALD cycles. The thickness of the ASD Ru layer on TiN is noted next to the corresponding number of Ru ALD cycles.

Defect mitigation solution by etching

The suppressed particle growth during the initial stages of EBE-CHRu/O$_2$ ALD enables a defect mitigation solution based on etching. Ru particles initially grow primarily by slow adsorption on the dielectric followed by adatom diffusion and coalescence, while the more rapid particle growth due to direct ALD on the particles only occurs when they reach critical size[22]. The initial suppression of particle growth gives rise to a window in which the Ru film thickness on TiN is higher as compared to the size of all defects on SiO$_2$. In this case, the defects can be fully etched while the Ru layer thickness is only partly affected.

This strategy is investigated on the 36nm hole patterns at 325°C (the upper limit of the ALD window) to make use of the enhanced Ru growth rate on TiN[24]. Table 1 shows the Ru layer thickness on TiN and the largest particle observed on SiO$_2$ for a variety of Ru ALD cycle numbers (SEM). These data show that the suppressed particle growth due to the size-dependent Ru nanoparticle reactivity effectively prevents defects from reaching the same size as the ASD Ru layer on TiN until a 3nm thin film has been grown. Afterwards, the diffusion-mediated growth and increased nanoparticle reactivity result in particles with sizes exceeding the selectively grown layer. For each ASD Ru thickness on TiN, a O$_2$/Cl$_2$ plasma etch was applied after DMA-TMS treatment and subsequent Ru ALD. An O$_2$ plasma etches Ru by forming volatile RuO$_4$, while addition of Cl$_2$ to the plasma enhances the etch rate[33]. Due to the size-dependent Ru nanoparticle reactivity, the etch efficacy depends strongly on the amount of Ru ALD cycles initially applied (Figure 4). For short processes yielding 1-3nm Ru layers on TiN after deposition, a 5s etch is sufficient to reduce defectivity on SiO$_2$ below the ToF-SIMS LOD. However for a 4nm layer, a much longer etch (15s) is needed, as for 5s and 10s residual defectivity is still detected by SF-SIMS. The much longer etch time can be explained by the much more rapid particle growth between 62 and 83 cycles compared to the initial stage, resulting in particle sizes exceeding the Ru layer thickness on TiN (Table 1). For each thickness an etch time was found for which no defects are detected by SF-SIMS. As a post-deposition etch step inevitably also attacks the Ru film grown on TiN, the integrity of the Ru layers on TiN will be evaluated further in this work during the discussion on TI patterning.

ALD cycles	Ru thickness on TiN [nm]	Largest particle radius [nm]
21	1	< 0.6 nm (LOD)
42	2	< 0.6 nm (LOD)
62	3	2.5
83	4	4.5

Table 1: Comparison between Ru layer thickness deposited on TiN and the largest particle observed on SiO_2 by SEM, after varying ALD cycle number at 325°C before applying an etch step
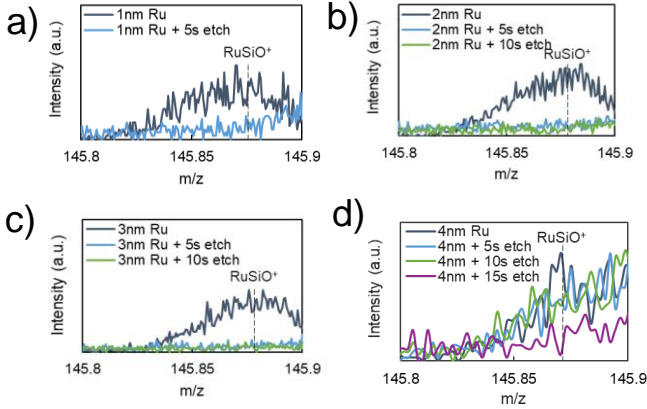
Figure 4: $RuSiO^+$ ion intensity before and after etch is presented for ASD at 325°C of a) 1nm Ru (21 cycles), b) 2nm Ru (42 cycles), c) 3nm Ru (62 cycles), d) 4nm Ru (83 cycles). Intensity data for the spectrum in d) are binned per three m/z channels for readability

Enhancing selectivity by limiting adsorption and surface diffusion

During the initial stages of $EBECHRu/O_2$ ALD on dielectrics, direct deposition on existing particles only occurs once particles reach a critical size of ~0.85nm, which they eventually achieve by adatom deposition followed by surface diffusion and coalescence. Surface diffusion can help to improve selectivity by moving material from the non-growth to the growth surface[23], but the diffusion length in $EBECHRu/O_2$ ALD is too small compared to the pattern dimensions to significantly mitigate defectivity as illustrated in the section discussing growth behaviour on SiO_2. Surface diffusion and aggregation are therefore undesirable at these pattern dimensions, as these phenomena are the primary initial driving force for particle growth. Particle growth can be suppressed by limiting adatom deposition on dielectrics, and by limiting surface diffusion to keep adatoms from aggregating into particles of critical size. In this work precursor adsorption on dielectrics and surface diffusion are limited by lowering the Ru ALD temperature from 325°C to 225°C. However, a decrease in ALD temperature can decrease the growth rate on both the dielectric non-growth surface and the TiN growth surface. We therefore investigate the impact of temperature on selectivity for the aforementioned defect mitigation strategy. The Ru ASD behaviour at 225°C was compared to the behaviour at 325°C to determine whether limiting surface diffusion on dielectrics can be exploited to reduce defectivity.

As the selectivity typically depends on the thickness of the selectively deposited layer, we compare defectivity on the dielectric for a specific Ru thickness on TiN rather than ALD cycle number. The Ru growth rate on TiN at 225°C is $0.2·10^{15}$ at cm^{-2} $cycle^{-1}$, two times lower as compared to the growth rate at 325°C (Figure 5a,b), which means that twice as many ALD cycles are needed to achieve the same thickness at 225°C compared to 325°C. Despite the significant increase in ALD cycles however, a significant decrease in

defectivity on the dielectric is observed. For a 4nm Ru layer on TiN, no Ru is measured by RBS on SiO_2 substrates at 225°C compared to $1.2·10^{15}$ at cm^{-2} at 325°C. The difference is also clearly observed in SEM both for non-patterned SiO_2 substrates and TiN/SiO_2 line patterns (Figure 5c). For both the patterned and non-patterned substrates, the dielectric surface transforms from defective with SEM coverages ranging between 7% and 17% at 325°C, to a situation where no defects are observed by SEM at 225°C. Nevertheless, direct precursor adsorption on the dielectric still occurs at 225°C, albeit at a lower rate compared to 325°C. The total amount of Ru deposited after 10 cycles was measured by Total X-Ray Fluorescence (TXRF). Particles are not expected to reach critical size by surface diffusion in the first 10 cycles, meaning that differences in Ru content can be attributed primarily to the differences in initial precursor adsorption rate on the $Si-CH_3$ terminated dielectric. We observe $5.3·10^{10}$ Ru at cm^{-2} after 10 cycles at 225°C compared to $23.8·10^{10}$ at cm^{-2} after 10 cycles at 325°C. The reduced adsorption rate and reduced surface diffusion result in significantly lower defectivity at 225°C compared to 325°C. SF-SIMS shows that while the defect level is significantly lower at 225°C, defects are still present (Figure 5d) and a post-deposition etch step would still be required. For the 225°C process however, the defects are smaller than the ~1nm SEM detection limit for an ASD-grown Ru layer of 4nm, and as such this strategy significantly facilitates the post-deposition etch. These results show that exploiting the $EBECHRu/O_2$ growth mechanism can effectively be used for defect mitigation during ASD on nanoscale patterns.
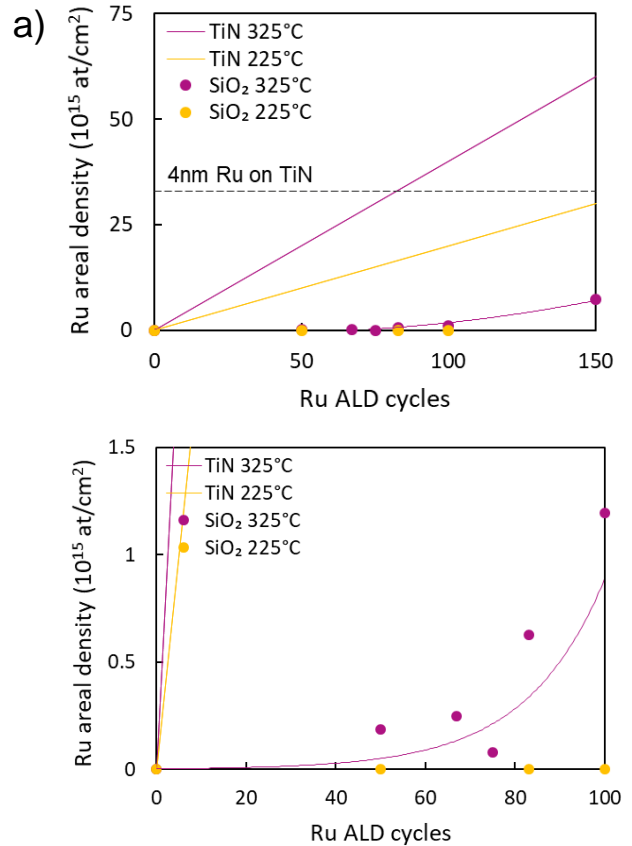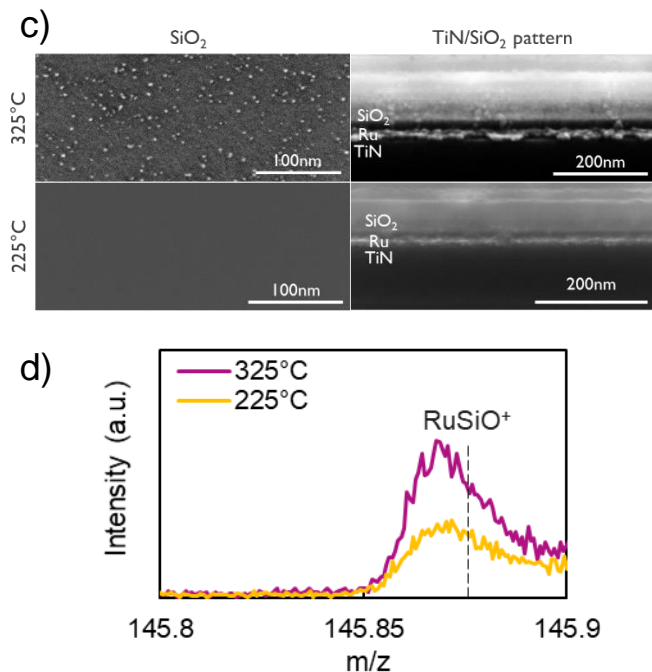
Figure 5: Comparison of Ru ASD at 325°C and 225°C by a) RBS on TiN and SiO$_2$ substrates, b) the same RBS data focused in the low areal density regime, c) SEM of SiO$_2$ substrates and TiN/SiO$_2$ nanopatterns after 83 Ru ALD cycles at 325°C or 150 Ru ALD cycles at 225°C, both corresponding to 4nm Ru ASD on TiN, d) SF-SIMS RuSiO$^+$ ion intensity after 62 Ru ALD cycles at 325°C or 125 Ru ALD cycles at 225°C, both on SiO$_2$. 83 and 150 Ru ALD cycles were chosen for the SEM images because the Ru film on TiN is easily distinguished for these cycle numbers, while 62 and 125 cycle numbers were chosen for SF-SIMS as these cycle numbers correspond to a 3nm Ru layer on TiN, which is the most promising condition for an ASD+etch strategy as identified in Table 1.

Bottom-up patterning enabled by Ru ASD

While a short O$_2$/Cl$_2$ etch is suitable to remove defects during the initial stages of EBECHRu/O$_2$ ASD, etching also attacks the selectively grown film. The previous sections illustrated how the size-dependent particle reactivity during EBECHRu/O$_2$ growth can be exploited to keep particles smaller compared to the selectively grown film. This allows the Ru particles to be fully removed without simultaneously removing the ASD pattern. This section evaluates whether a window exists in which no more defects are observed by SF-SIMS, while the pattern integrity resulting from Ru ASD remains unaffected. If defectivity is insufficiently removed during etch, residual defects on SiO$_2$ will lead to undesired masking during TI patterning (Figure 6a). If on the other hand the Ru etch is too long, the Ru ASD pattern integrity is affected and is no longer functional (Figure 6b). As both effects are easily observed in plan-view SEM after TI patterning, TI is used to probe the potential for Ru ASD to generate a functional pattern.

The potential of Ru ASD for TI was investigated using 36nm hole patterns, as these are relevant for the definition of interconnect features in nanoelectronic device fabrication[30]. Substrates were DMA-TMS treated and subsequently received varying numbers of Ru ALD cycles at 325°C corresponding to 1-4nm nominal Ru thickness on TiN. After ASD, TI was carried out by wet SiO$_2$ removal in buffered HF solution (bHF) which exposes the buried

TiN/Si$_3$N$_4$ line pattern except in those places where Ru was deposited. The obtained pattern was then transferred down by etching the exposed TiN. For all investigated Ru layer thicknesses, a continuous Ru layer on TiN effectively protects the underlying TiN during the pattern transfer etch (Figure 6a). The problem of defectivity becomes apparent when the patterns before (Figure 3a) and after (Figure 6a) TI are compared, showing how the Ru defects on SiO$_2$ result in excessive unwanted local protection of the underlying TiN. Since an increasing number of Ru ALD cycles results in increasing defectivity, the pattern obtained after TI strongly diverges from the initial hole patterns for the thicker layers. Inversely, for the thinnest (1nm) layer, the pattern after TI matches the initial pattern almost perfectly, illustrating the potential of ASD for tone inversion patterning. However, defects can still be observed albeit very sparsely (~10^8 cm^{-2}), and these defects negatively affect the performance of the resulting devices. Defect mitigation is therefore required to obtain a functional pattern.

These results are now compared to patterns on which a Ru defect etch was applied after ASD. For each condition where the defectivity is below the ToF-SIMS LOD, the samples were subjected to TI patterning to validate the Ru pattern integrity. For the thinnest layers, the short defect etch unfortunately also removes or damages the Ru pattern (Figure 6b). However a window exists at an ASD Ru layer of 3nm (62 cycles) followed by a 5s defect etch, in which defectivity is fully removed to below the ToF-SIMS LOD while the Ru pattern remains intact and the Ru layer effectively protects the underlying TiN (Figure 6c). As a result, no defects were observed in the pattern after TI. Figure 6d and 6e show the defectivity on SiO$_2$ before and after Ru defect etch, respectively in the centre and each cardinal direction of a 300mm wafer. This illustrates that the defect etch is effective across large-area substrates of industrial relevance. For an initial Ru ASD thickness of 4nm (83 cycles) the Ru layer on TiN is fully removed before defectivity is fully mitigated. These findings are in agreement with the Ru morphology on these nanopatterns listed in Table 1, as all defects are smaller compared to the ASD Ru layer on TiN during the early stage (up to 62 cycles), while later in the growth evolution (83 cycles) this is no longer the case as particle coalescence and size-dependent particle reactivity ensure that particles become too large to selectively remove.

c)

d)

400nm

e)

400nm
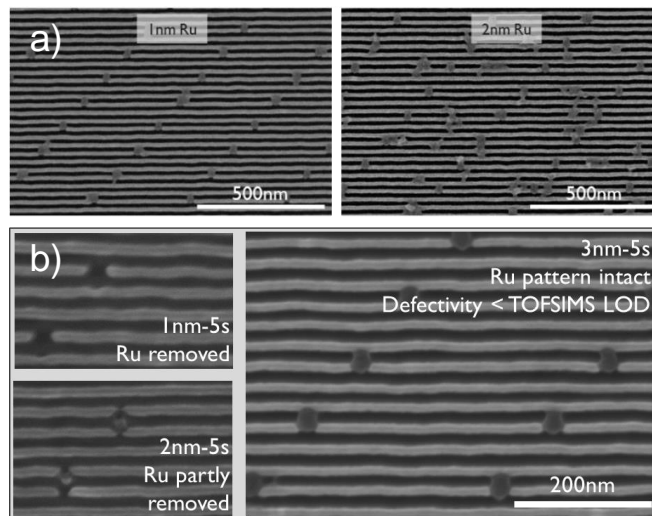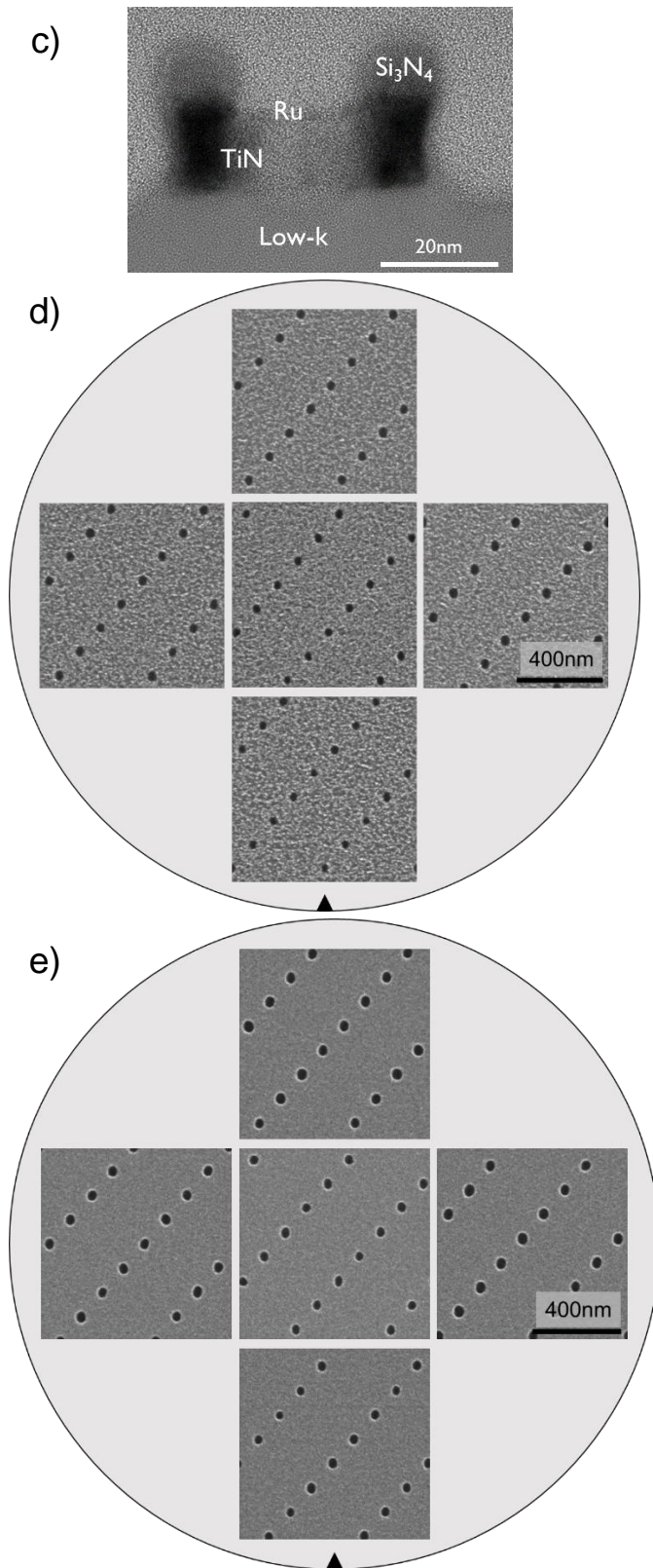
Figure 6: TI patterning is demonstrated using area-selective Ru ALD at 325°C on TiN/SiO$_2$ patterns. a) plan-view SEM after TI patterning for 1nm (21 cycles), 2nm (42 cycles), and 4nm (83 cycles) Ru ASD without defect etch b) plan-view SEM after TI patterning for 1nm, 2nm, and 3nm (62 cycles) Ru ASD and 5s post-

deposition Ru defect etch c) cross-view TEM of an ASD Ru layer corresponding to 3nm Ru ASD followed by a 5s post-deposition Ru defect etch d) Top-view SEM of various locations on 300mm wafers after 3nm Ru ASD (62 cycles) before Ru defect etch e) Top-view SEM of the same locations after Ru defect etch

These results show that when the EBECHRu/O$_2$ growth mechanism is exploited, Ru ASD enabled by a DMA-TMS pretreatment and a post-deposition etch step can yield a functional TI pattern with no defects being detected even by the most surface-sensitive techniques. Specifically, the distinct growth behaviour of EBE-CHRu/O$_2$ ALD on dielectrics in the initial regime enables the possibility of etching defects while they are still significantly smaller compared to the ASD-grown film.

Conclusion

This work simultaneously demonstrates a Ru ASD process with a defect mitigation solution and the application of this ASD process in bottom-up nanopatterning, both of which are highly relevant for industrial applications. We have designed a defect mitigation strategy for ASD based on the size-dependent reactivity of Ru nanoparticles. During the initial stages of EBECHRu/O$_2$ ALD, this size-dependent Ru particle reactivity suppresses defect growth, keeping defects smaller compared to the thickness of the selectively grown film. This results in a window in which the defects can be etched with limited impact on the selectively grown film. We demonstrate a Ru ASD process on TiN selective to SiO$_2$ for which no defects are observed by SF-SIMS, which is among the most surface-sensitive techniques. This Ru ASD process yields a functional pattern in 36nm features across 300mm wafers.

Pattern surface composition, dimensions, and topography can play an important role in ASD on nanopatterns, especially for diffusion-mediated growth processes. For the EBECHRu/O$_2$ ALD on the nanopatterns considered here, the diffusion length is limited compared to the feature dimensions. At smaller feature sizes, surface diffusion could be used to move material from the non-growth surface to the growth surface, providing another viable strategy to enhance selectivity.

Bottom-up patterning becomes critical in nanoelectronics device fabrication as feature dimensions go down, and defectivity is one of the main roadblocks for ASD-based solutions. In addition to bottom-up patterning, ASD of ruthenium is important for several other applications including the production of core-shell catalytic nanoparticles and nano-interconnects. The ASD process and defect mitigation strategy as described here provide an excellent starting point for the development of cyclic passivation-deposition-etch processes, where each cycle increases the thickness of the selectively deposited layer. Such processes become increasingly relevant for applications which require high thickness of selective bottom-up metal such as nano-interconnects. Ru ASD is highly relevant for this application, as Ru outperforms Cu as a conductor both in terms of resistivity and reliability at the nanoscale.

The defect mitigation approach followed in this work can potentially be extended to other systems with size-dependent nanoparticle reactivity, including most (noble) metals. This work also motivates the further investigation into growth mechanisms and their impact on ASD, to contribute to the development of defect mitigation solutions for other area selective deposition processes.

Experimental Details

All experiments were performed on 300mm Si(100) wafers covered with 100nm thermally grown SiO$_2$. Figure 7 provides an overview of each substrate used throughout this study. TiN substrates were obtained by Physical Vapor Deposition (PVD) using a Ti tar-

7

get and N_2 ambient in an AMAT Endura PVD chamber. SiO_2 substrates were obtained by Plasma-Enhanced ALD (PEALD) at 75°C using an ASM Eagle 12 chamber. To obtain TiN/SiO_2 line patterns (Figure 7c), 25nm PVD TiN was deposited followed by 75nm PEALD SiO_2. Patterning was achieved by depositing 100nm SOC, 30nm spin-on-glass (SOG), 29nm Anti-Reflective Coating (ARC), and 105nm photoresist (PR) in an ASML Twinscan NXT:1950i 193nm immersion scanner, followed by lithographic patterning of line/space patterns. After pattern definition, trenches were etched into the SiO_2 layer landing on TiN followed by in-situ strip of the PR/SOG/SOC layers. SiO_2 was etched by CF_4/CHF_3, while in situ strip was performed by O_2 plasma. Finally a wet clean was applied to TiN/SiO_2 patterns to remove CF_x residues from etch. The fabrication method for TiN/SiO_2 hole patterns with buried Si_3N_4 lines (Figure 7d) is discussed elsewhere[30]. In the TiN/SiO_2 hole patterns, the Si_3N_4 lines are buried during ASD and are only exposed during TI patterning after ASD, and serve only to define the underlying pattern for the application.
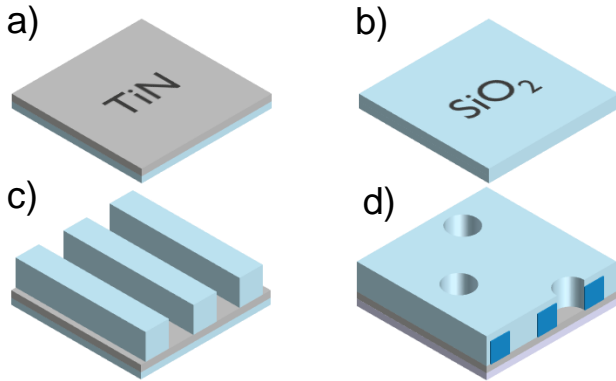
Figure 7: Overview of the substrates used throughout this work. a) 15nm TiN, b) 15nm SiO_2, c) 54nm wide TiN/SiO_2 line patterns produced by etching trenches in SiO_2 exposing TiN on bottom, d) TiN/SiO_2 structures used in TI patterning, with 36nm-90μm wide holes in SiO_2 partly exposing the TiN underlayer. Si_3N_4 (dark blue) and low-k dielectric (lilac) are buried during ASD, and are only used after ASD to demonstrate the TI patterning process (Figure 9).

Figure 8 illustrates both types of TiN/SiO_2 nanopatterns used in this study. The line patterns are shown in Figure 8a. SiO_2 lines are 37nm wide and alternate with 54nm wide TiN lines residing at the bottom of each trench. Trench depth is measured at 70nm. The hole patterns used to demonstrate TI are shown in Figure 8b. Holes with 36nm-90μm lateral dimensions are etched in a 35nm thick SiO_2 layer, the smallest of which (36nm) are illustrated in the figure.
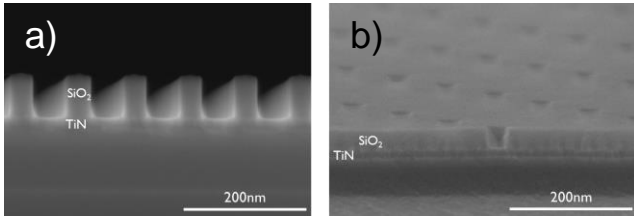
Figure 8: a) cross-view SEM of 54nm TiN/SiO_2 line patterns, b) cross-view SEM of 36nm TiN/SiO_2 hole patterns for Tone Inversion

Ru ASD was performed by a DMA-TMS surface pretreatment step followed by Ru ALD. DMA-TMS is used to enable Ru ASD on TiN vs SiO_2, as aminosilanes can selectively inhibit growth on dielectric surfaces[7,8,12]. The pretreatment is carried out in a TEL Tactras system and consists of a thermal desorption step followed by a vapour-phase treatment. First the substrate is kept in the closed reactor chamber in 5 Torr N_2 ambient at 250°C for 10 minutes to desorb residual moisture and organics. Afterwards the reactor is evacuated and filled with a mixture of 500sccm DMA-TMS and 350sccm N_2 up to a pressure of 5 Torr. The substrates are kept in this mixture for 300s to saturate the surface reactions. Ru ALD was performed at 325°C and 225°C in an ASM Pulsar 3000 cross-flow reactor connected to a Polygon platform. Substrates were sequentially exposed to alternating pulses EBECHRu and O_2, separated by N_2 purges. The exposure times were 5s EBECHRu, 5s N_2, 0.4s O_2, 3s N_2 in each case. On some substrates a short Ru etch was applied after ASD to reduce defectivity on the SiO_2 before continuing with the remaining Tone Inversion steps. Ru etching was carried out using a zero bias O_2/Cl_2 plasma in a LAM Versys chamber at 60°C with varying etch times.

Tone Inversion patterning was performed on substrates with 36nm-90μm TiN/SiO_2 hole patterns after Ru ASD (Figure 9). First the substrates were treated with bHF to remove the sacrificial SiO_2, exposing the buried Si_3N_4 lines and remaining TiN (Figure 9c). The bHF solution was prepared by combining solutions of 40% NH_4F and 49% HF in a 7:1 volume ratio. After SiO_2 removal, the pattern transfer into the TiN layer was performed by a two-step dry etch. First, the TiN surface oxide is opened using 10s BCl_3, and the TiN is subsequently etched using $Cl_2/N_2/C_2H_4$ for 22s. This etch step opens the TiN where it is not protected by Si_3N_4 lines or the selectively deposited Ru layer (Figure 9d).
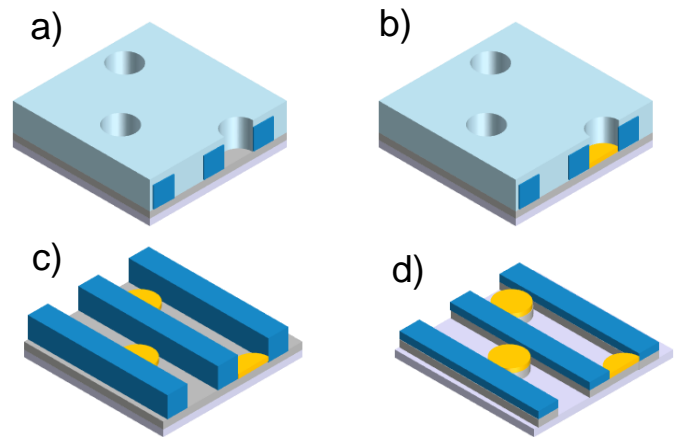
Figure 9: Process for nanopatterning by ASD-enabled Tone Inversion (TI). In TI, a pattern is obtained by etching features in a soft material and filling those features with hard material. This is typically more straightforward than patterning the hard material directly. a) a regular line pattern of Si_3N_4 spacers (dark blue) is created on TiN (grey) by Self-Aligned Quadruple Patterning (SAQP). The entire structure is then covered by sacrificial SiO_2 (light blue) and a hole pattern is etched. b) selective deposition of a Ru layer on TiN inside the holes. c) SiO_2 removal by bHF d) pattern transfer into TiN by dry etching, exposing underlying low-k dielectric (lilac).

Substrates were characterized before and after Ru ASD, Ru defect etching, and Tone Inversion using a variety of chemical and morphological techniques. SEM was used to measure pattern dimensions, the thickness of the deposited layer on TiN, and the density and size distribution of Ru defects on SiO_2. SEM was performed with a Hitachi SU8000 microscope using a 10 kV/10 μA incoming beam and a secondary electron detector, which can measure Ru particle sizes down to $1nm^2$. Particle radii were extracted from SEM micrographs using the ImageJ software package. In

some cases the Ru morphology after ASD was studied by TEM using a Titan^3 G2 60-300 operated at 120kV, for which samples were coated with SOC followed by Pt before liftout. The total amount of deposited Ru on each substrate was characterized either by RBS using a 1.523 MeV He$^+$ incoming ion beam and a silicon surface barrier detector for analysis, or by TXRF using a Rigaku TXRF300 tool with a 24 keV beam to quantify Ru areal density. ToF-SIMS was used to characterize surface species with a ION-TOF GmbH ToF-SIMS IV instrument using a 25kV Bi^{3+} analysis beam. Ru defectivity on patterned substrates was measured using SF-SIMS. SF-SIMS uses the principle that in SIMS, charged clusters consisting of multiple atoms are primarily generated when those atoms are in close proximity on the sample[18]. As the Ru$^+$ signal from our samples can originate both from Ru on SiO$_2$ and Ru on TiN, the Ru contribution from defectivity on SiO$_2$ is isolated by following the RuSiO$^+$ cluster.

REFERENCES

[1]   R. Clark, K. Tapily, K. H. Yu, T. Hakamata, S. Consiglio, D. O'Meara, C. Wajda, J. Smith, G. Leusink, *APL Mater.* **2018**, *6*, DOI 10.1063/1.5026805.

[2]   A. J. M. Mackus, A. A. Bol, W. M. M. Kessels, *Nanoscale* **2014**, *6*, 10941.

[3]   K. Yan, Z. Lu, H.-W. Lee, F. Xiong, P.-C. Hsu, Y. Li, J. Zhao, S. Chu, Y. Cui, *Nat. Energy* **2016**, *1*, 16010.

[4]   F. S. Minaye Hashemi, C. Prasittichai, S. F. Bent, *ACS Nano* **2015**, *9*, 8710.

[5]   T. Ishizaka, T. Sakuma, M. Kawamata, O. Yokoyama, T. Kato, A. Gomi, C. Yasumuro, H. Toshima, T. Fukushima, Y. Mizusawa, T. Hatano, M. Hara, *Microelectron. Eng.* **2012**, *92*, 76.

[6]   A. Mameli, M. J. M. Merkx, B. Karasulu, F. Roozeboom, W. M. M. Kessels, A. J. M. MacKus, *ACS Nano* **2017**, *11*, 9303.

[7]   T. D.-M. Elko-Hansen, J. G. Ekerdt, *ECS Trans.* **2017**, *80*, 29.

[8]   Y. Au, Y. Lin, H. Kim, E. Beh, Y. Liu, R. G. Gordon, *J. Electrochem. Soc.* **2010**, *157*, D341.

[9]   E. Stevens, Y. Tomczak, B. T. Chan, E. Altamirano Sanchez, G. N. Parsons, A. Delabie, *Chem. Mater.* **2018**, *30*, 3223.

[10]   B. Kalanyan, P. C. Lemaire, S. E. Atanasov, M. J. Ritz, G. N. Parsons, *Chem. Mater.* **2016**, *28*, 117.

[11]   M. M. Minjauw, H. Rijckaert, I. Van Driessche, C. Detavernier, J. Dendooven, *Meet. Abstr.* **2018**, *MA2018-02*, 984.

[12]   R. Khan, B. Shong, B. G. Ko, J. K. Lee, H. Lee, J. Y. Park, I. K. Oh, S. S. Raya, H. M. Hong, K. B. Chung, E. J. Luber, Y. S. Kim, C. H. Lee, W. H. Kim, H. B. R. Lee, *Chem. Mater.* **2018**, *30*, 7603.

[13]   J.-C. Chiou, K. Juang, M. Chen, *J. Electrochem. Soc.* **1995**, *142*, 177.

[14]   A. J. M. Mackus, in *2018 Int. Symp. VLSI Technol. Syst. Appl.*, IEEE, **2018**, pp. 1–2.

[15]   R. Vallat, R. Gassilloud, B. Eychenne, C. Vallée, *J. Vac. Sci. Technol. A Vacuum, Surfaces, Film.* **2017**, *35*, 01B104.

[16]   M. A. Douglas, P. J. Chen, *Surf. Interface Anal.* **1998**, *26*, 984.

[17]   V. Spampinato, S. Armini, A. Franquet, T. Conard, P. van der Heide, W. Vandervorst, *Appl. Surf. Sci.* **2019**, *476*, 594.

[18]   A. Franquet, B. Douhard, D. Melkonyan, P. Favia, T. Conard, W. Vandervorst, *Appl. Surf. Sci.* **2016**, *365*, 143.

[19]   R. L. Puurunen, W. Vandervorst, *J. Appl. Phys.* **2004**, *96*, 7686.

[20]   M. A. Alam, M. L. Green, *J. Appl. Phys.* **2003**, *94*, 3403.

[21]   F. Grillo, H. Van Bui, J. A. Moulijn, M. T. Kreutzer, J. R. Van Ommen, *J. Phys. Chem. Lett.* **2017**, *8*, 975.

[22]   J. Soethoudt, F. Grillo, E. A. Marques, J. R. van Ommen, Y. Tomczak, L. Nyns, S. Van Elshocht, A. Delabie, *Adv. Mater. Interfaces* **2018**, 1800870.

[23]   J.-O. Carlsson, *Crit. Rev. Solid State Mater. Sci.* **1990**, *16*, 161.

[24]   M. Popovici, B. Groven, K. Marcoen, Q. M. Phung, S. Dutta, J. Swerts, J. Meersschaut, J. A. Van Den Berg, A. Franquet, A. Moussa, K. Vanstreels, P. Lagrain, H. Bender, M. Jurczak, S. Van Elshocht, A. Delabie, C. Adelmann, *Chem. Mater.* **2017**, *29*, 4654.

[25]   B. Briggs, C. J. Wilson, K. Devriendt, M. H. van der Veen, S. Decoster, S. Paolillo, J. Versluijs, E. Kesters, F. Sebaai, N. Jourdan, Z. El-Mekki, N. Heylen, P. Verdonck, D. Wan, O. V. Pedreira, K. Croes, S. Dutta, J. Ryckaert, A. Mallik, S. Lariviere, J. Bommels, Z. Tokei, in *2017 IEEE Int. Interconnect Technol. Conf.*, IEEE, **2017**, pp. 1–3.

[26]   S. J. Holmes, C. Tang, S. Burns, Y. Yin, R. Chen, C. Koay, S. Kini, H. Tomizawa, S.-T. Chen, N. Fender, B. Osborn, L. Singh, K. Petrillo, G. Landie, S. Halle, S.

Liu, J. C. Arnold, T. Spooner, R. Varanasi, M. Slezak, M. Colburn, S. Dunn, D. Hetzer, S. Kawakami, J. Cantone, in *2011 IEEE/SEMI Adv. Semicond. Manuf. Conf.*, IEEE, **2011**, pp. 1–8.

[27] J. C. Arnold, S. Burns, S. K. Kanakasabapathy, Y. Yin, *Self Aligning via Patterning*, **2011**.

[28] H. He, C. Liu, A. Reznicek, C. Tseng, T. Yamashita, *Tone Inverted Directed Self-Assembly (DSA) Fin Patterning*, **2015**.

[29] M. A. Guillorn, S. J. Holmes, C. Liu, H. Miyazoe, H. Tsai, *Tone Inversion of Self-Assembled Self-Aligned Structures*, **2012**.

[30] B. Briggs, J. Versluijs, J. Bommels, C. J. Wilson, Z. Tokei, A. Mallik, J. Soethoudt, in *2018 China Semicond. Technol. Int. Conf.*, IEEE, **2018**, pp. 1–4.

[31] F. Ren, S. J. Pearton, J. R. Lothian, C. R. Abernathy, W. S. Hobson, *Cit. J. Vac. Sci. Technol. B Microelectron. Nanom. Struct. Process.* **1992**, *10*, 2407.

[32] M. Haverlag, G. M. W. Kroesen, C. J. H. De Zeeuw, Y. Creyghton, T. H. J. Bisschops, F. J. De Hoog, M. Haveriag,) Y Creyghton, *Cit. J. Vac. Sci. Technol. B Microelectron. Process. Phenom.* **1989**, *7*, 529.

[33] H. W. Kim, J.-H. Han, B.-S. Ju, C.-J. Kang, J.-T. Moon, *Study of Ru Etching Using O 2 /Cl 2 Helicon Plasmas*, **n.d.**